AGU PUBLICATIONS

JGR

Journal of Geophysical Research: Atmospheres

RESEARCH ARTICLE

10.1002/2014JD021940

Influence of ice sheet topography on Greenland precipitation during the Eemian interglacial

N. Merz[1,2], G. Gfeller[1,2], A. Born[1,2], C. C. Raible[1,2], T. F. Stocker[1,2], and H. Fischer[1,2]

[1]Climate and Environmental Physics, University of Bern, Bern, Switzerland, [2]Oeschger Centre for Climate Change Research, University of Bern, Bern, Switzerland

Key Points:
- A modified Greenland ice sheet results in distinct local precipitation changes
- Moisture availability and weather patterns are insensitive to topography changes
- Topography changes can affect moisture transport to Greenland ice core sites

Correspondence to:
N. Merz,
merz@climate.unibe.ch

Citation:
Merz, N., G. Gfeller, A. Born, C. C. Raible, T. F. Stocker, and H. Fischer (2014), Influence of ice sheet topography on Greenland precipitation during the Eemian interglacial, *J. Geophys. Res. Atmos.*, *119*, 10,749–10,768, doi:10.1002/2014JD021940.

Received 25 APR 2014
Accepted 31 AUG 2014
Accepted article online 5 SEP 2014
Published online 24 SEP 2014

Abstract Greenland precipitation and its relationship to the synoptic forcing has been studied for the last interglacial period (i.e., the Eemian) using a set of global climate simulations. We distinguish between precipitation changes due to the Eemian orbital forcing and responses to modifications in the Greenland ice sheet (GrIS) topography. Precipitation changes caused by orbital forcing alone are of moderate amplitude and are largely determined by large-scale changes in moisture availability. In contrast, changes in GrIS topography lead to distinct precipitation anomalies over Greenland, while the effect on far-field regions is negligible. The analysis of the simulations reveals the control of the GrIS topography on where moist air masses are orographically lifted and cause substantial precipitation. However, the general moisture availability and the moisture transport associated with typical weather situations remain unchanged in all simulations. A focal point of the study is precipitation at pNEEM, i.e., the suggested deposition site of Eemian ice archived in the North Greenland Eemian ice drilling project (NEEM) ice core. Eemian orbital forcing leads to an increase in summer precipitation at pNEEM, whereas changes in the GrIS topography can result in either increased or decreased precipitation. Transport routes prior to precipitation events at pNEEM show that moisture is predominantly advected from westerly to southerly directions as the GrIS acts as an impassable barrier for easterly moisture transport. One scenario of Eemian melting of northeastern Greenland, however, allows moist air masses from the Norwegian Sea to arrive at pNEEM. Consequently, this GrIS topography would result in transport-related changes of Eemian wet-deposited aerosol records.

1. Introduction

Studies of past interglacial periods provide valuable information concerning the response of the Greenland ice sheet (GrIS) to warm climate conditions. In this respect, the last interglacial (circa 130–115 ka B.P.), known as the Eemian, is the best documented period. The Eemian was characterized by high summer insolation that caused warmer than present conditions in the high latitudes of both hemispheres. Evidence from fossil coral reefs suggests an Eemian sea level high stand of 6 to 9 m above present [*Kopp et al.*, 2009], which would require considerable melting from the polar ice caps. At the same time, the presence of Eemian and older ice in several Greenland ice cores [e.g., *Dansgaard et al.*, 1985; *Willerslev et al.*, 2007; *North Greenland Ice Core Project members*, 2004; *North Greenland Eemian ice drilling project (NEEM) community members*, 2013] indicates that a substantial part of the GrIS survived the last interglacial, but precise estimates of the Eemian size and shape of the GrIS do not exist due to the lack of proxy data. Hence, the response of the GrIS topography to Eemian climate conditions has been estimated through ice sheet modeling efforts [e.g., *Cuffey and Marshall*, 2000; *Otto-Bliesner et al.*, 2006; *Robinson et al.*, 2011; *Born and Nisancioglu*, 2012; *Stone et al.*, 2013; *Helsen et al.*, 2013]. However, the resulting GrIS topographies and estimated contributions to the sea level high stand reveal large uncertainties ranging from almost no melting to a contribution of over 5 m sea level rise [*Robinson et al.*, 2011; *Cuffey and Marshall*, 2000]. Moreover, different modeling studies do not agree on whether melting predominantly occurred in southern [*Cuffey and Marshall*, 2000; *Otto-Bliesner et al.*, 2006] or northern Greenland [*Born and Nisancioglu*, 2012; *Stone et al.*, 2013].

The local climate of Greenland is known to be closely tied to its ice sheet, which largely determines the surface elevation profile [*Ohmura and Reeh*, 1991; *Ettema et al.*, 2010]. At present, Greenland's topography is marked by steep slopes along the ice sheet margins and a relatively flat, high plateau made up of the North and South Dome of the GrIS. The high-altitude and the highly reflective ice surface in central Greenland lead to very cold and dry conditions throughout the year. In contrast, coastal areas are warmer (particularly in southern Greenland) and receive a considerable amount of precipitation when passing cyclones create

onshore flow of moist air masses that are eventually lifted by the steep margins of the GrIS [*Chen et al.*, 1997; *Schuenemann et al.*, 2009]. As the orography forces low-level air masses to ascend, they can cool adiabatically as they rise in altitude. If these air masses are moist, this results in cloud formation and, subsequently, local precipitation. The orographic uplift leads to immediate precipitation prohibiting moist air masses from reaching Greenland's interior, which lies leeward of the orographic barrier and builds the so-called dry slot [*Roe*, 2005]. In addition, the presence of the Greenland anticyclone [*Hobbs*, 1945] over the GrIS induced by the descending air masses over the cold ice sheet also prevents onshore flow of moist air masses from entering the plateau area.

The significant retreat of the GrIS during the Eemian resulting in a reduced extent and/or height of the ice sheet leads to a weakening of the Greenland anticyclone [*Hakuba et al.*, 2012; *Merz et al.*, 2014]. Hence, the impact of a reduced GrIS on Greenland precipitation is twofold: the weaker anticyclone leads to more direct flow toward the GrIS topography, thus resulting in increased upstream and reduced downstream precipitation [*Hakuba et al.*, 2012]. At the same time, the reduction in orography itself makes it easier for moist air masses to penetrate farther inland and precipitate over the Greenland plateau. The presence of the ice sheet has also various effects on the atmospheric flow and climate in the vicinity of Greenland as shown by several model experiments, investigating the impact of a complete removal of Greenland [e.g., *Kristjansson and McInnes*, 1999; *Dethloff et al.*, 2004; *Petersen et al.*, 2004; *Junge et al.*, 2005; *Tsukernik et al.*, 2007; *Kristjansson et al.*, 2009]. Identified large-scale effects involve modifications of the North Atlantic stationary wave field [*Junge et al.*, 2005] and the North Atlantic storm track [*Petersen et al.*, 2004; *Dethloff et al.*, 2004; *Junge et al.*, 2005]. Moreover, important effects have been observed with respect to local cyclone evolution [e.g., *Kristjansson and McInnes*, 1999; *Tsukernik et al.*, 2007; *Kristjansson et al.*, 2009]. For example, Greenland's orography accounts for lee cyclogenesis east of southern Greenland strengthening the Icelandic low [*Kristjansson and McInnes*, 1999; *Tsukernik et al.*, 2007]. Furthermore, winter cyclones that typically approach from the southwest experience a "bifurcation," i.e., a splitting of the cyclone tracks at the southern tip of Greenland [*Chen et al.*, 1997; *Tsukernik et al.*, 2007].

In this study, we analyze the impact of a reduced GrIS on Greenland precipitation during Eemian climate conditions using a comprehensive climate model. In contrast to previous studies using idealized reductions of the GrIS, we implement GrIS masks that are results of two recent ice sheet modeling efforts for the Eemian [*Robinson et al.*, 2011; *Born and Nisancioglu*, 2012]. These topographies are constrained by present and paleo-information and, thus, can be regarded as possible scenarios of how Greenland might have looked during the last interglacial. This study is subsequent work to *Merz et al.* [2014], in which the response of the Greenland surface climate in terms of temperature, surface winds, and surface energy balance to the same set of Eemian GrIS topographies was investigated. The simulated precipitation response to variations in the GrIS topography is compared with changes in the hydrological cycle due to the Eemian orbital forcing, emphasizing that the precipitation sensitivity to GrIS topography is of great relevance. Hence, the results of this study are a valuable addition to the state of the art Eemian modeling studies [e.g., *Nikolova et al.*, 2013; *Lunt et al.*, 2013], which neglect the effect of a reduced GrIS.

Furthermore, we investigate whether changes in the moisture sources or in the moisture transport precede the simulated changes in Greenland moisture deposition (i.e., precipitation). For a thorough understanding of the connection between Greenland precipitation and the atmospheric circulation, analysis on an event-by-event basis on a daily time scale is required [*Schuenemann et al.*, 2009]. Accordingly, we assess the synoptic forcing of the precipitation changes identified in the Eemian simulations by retrieving typical (daily) Greenland weather patterns through circulation-type classification based on a cluster analysis technique. A second focus of the study lies on precipitation changes at the so-called pNEEM location, i.e., the suggested deposition site of Eemian ice archived in the North Greenland Eemian ice drilling project (NEEM) ice core (camp site at 77.5°N/50.9°W, 2443 m above sea level) [*NEEM community members*, 2013]. The Eemian ice obtained from the NEEM core makes this currently the only Greenland ice core archive covering the entire last interglacial period. Thus, an improved understanding of the processes relevant to the local climate at pNEEM during the Eemian is of particular interest. With the aid of the weather pattern analysis we show which synoptic situations are important for precipitation recorded at pNEEM. In addition, we use Lagrangian back trajectory analysis to determine the moisture transport toward the pNEEM site and assess how the moisture transport routes depend on the Eemian GrIS topography. The corresponding results are of importance for the interpretation of Eemian proxy records that are closely related to accumulation or wet deposition.

Table 1. List of Model Simulations (One Present Day, One Preindustrial, and Five Eemian Simulations) and the External Forcings Used in These Experiments[a]

Simulation	Orbital Parameters	SST/Sea Ice	CO_2 (ppm)	CH_4 (ppb)	N_2O (ppb)	TSI (W m^{-2})	Ice sheets
PD	pd	pd	354	1694	310	1361.8	pd
PI	pd	pi	280	760	270	1360.9	pd
EEMpd	125 ka	125 ka	272	622	259	1360.9	pd
EEMr1	125 ka	125 ka	272	622	259	1360.9	EEMr1
EEMr2	125 ka	125 ka	272	622	259	1360.9	EEMr2
EEMr3	125 ka	125 ka	272	622	259	1360.9	EEMr3
EEMr4	125 ka	125 ka	272	622	259	1360.9	EEMr4

[a]Present-day levels are denoted as pd and preindustrial levels as pi, respectively. SST and sea ice fields are obtained from corresponding fully coupled CCSM3 simulations (see *Merz et al.* [2014] for details). GHG values correspond to the Paleoclimate Modelling Intercomparison Project protocol. Solar forcing is expressed as total solar irradiance (TSI) and corresponds to CCSM4 standard levels. The set of implemented ice sheets is shown in Figure 1.

In the following section we give an overview over the experimental setup and the methods used in the analysis. In sections 3 and 4 we present the Greenland precipitation patterns as simulated for preindustrial and Eemian climate and their response to changes in GrIS topography. Subsequently, the role of synoptic weather situations is described in section 5. Changes in precipitation and in the moisture transport relevant for pNEEM are presented in section 6, and the implications for corresponding NEEM proxy records are discussed in section 7. Finally, a summary and conclusions are given in section 8.

2. Data and Methods

2.1. Climate Simulations

This study uses time-slice simulations performed with the Community Climate System Model version 4 (CCSM4) [*Gent et al.*, 2011] in a horizontal resolution of 0.9° × 1.25° (corresponding to a grid cell size of approximately 100 × 50 km at 70°N). The model is run with the atmosphere-land-only setup, i.e., interactive atmosphere and land surface but no dynamic representation of the ocean and sea ice. Instead, monthly mean sea ice cover and sea surface temperatures (SSTs) are prescribed as lower boundary conditions. To account for the different states of the ocean, we use sea ice and SST fields which are obtained from lower resolved but fully coupled CCSM3 simulations of the respective time period (Eemian [*Bakker et al.*, 2013], preindustrial [*Merkel et al.*, 2010], and present day [*Hofer et al.*, 2011]). These so-called Atmospheric Model Intercomparison Project (AMIP)-type simulations are very cost efficient compared to a fully coupled setup. This allows us to perform a set of time-slice simulations with a fairly high horizontal resolution that are appropriate for studying regional atmospheric changes in Greenland. As a drawback, these simulations do not allow feedbacks with the ocean and sea ice components. A detailed technical description of this CCSM4 AMIP-type model setup can be found in *Evans et al.* [2013], and a specific evaluation of the atmospheric component is further provided by *Neale et al.* [2013].

A total of seven experiments are performed: a present-day (PD) simulation, a preindustrial (PI) simulation, and five Eemian (EEM) simulations differing in the implemented GrIS topography. In each simulation the external forcing is held constant throughout the time of simulation (33 years, of which the last 30 years are used for the analysis). Hence, the PD simulation is run with perpetual 1990 A.D. conditions whereas PI equivalently uses perpetual forcing for 1850 A.D., and the five EEM simulations use perpetual 125 ka conditions. An overview of the simulations and the most important external forcing factors (e.g., greenhouse gas (GHG) concentrations, orbital, and solar forcing) is given in Table 1. Note that the PD simulation has previously been used and described in *Merz et al.* [2013], and a detailed presentation of the PI and all EEM simulations is provided in *Merz et al.* [2014]. Consequently, only a brief summary of the major simulation settings is given here.

The five EEM simulations differ in the implemented height and extent of the GrIS. The resulting topographies are shown in Figure 1. EEMpd is the reference simulation using Eemian external forcing but the present-day topography. Climate anomalies associated with the Eemian orbital forcing are computed as the difference EEMpd − PI. In order to isolate the effect of a reduced GrIS, EEMpd is further compared with the four other Eemian simulations which include a smaller (in terms of extent) and lower (in terms of height)

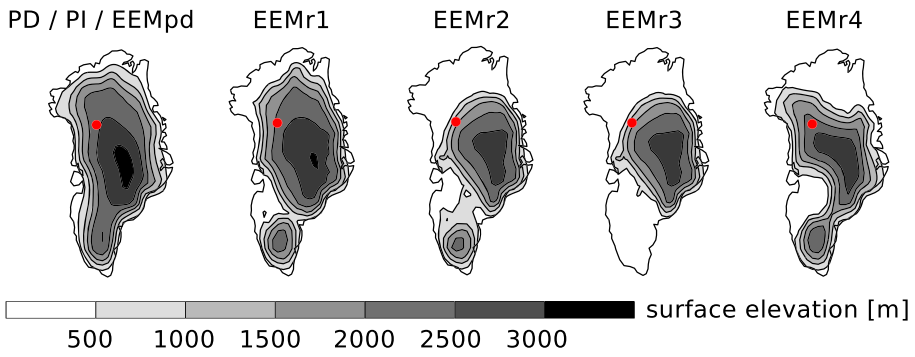

Figure 1. Eemian Greenland ice sheet surface elevations (m) implemented in the model simulations. The red dot indicates the location of pNEEM (suggested deposition site of Eemian ice found in the NEEM ice core).

ice sheet (Figure 1). These different Eemian GrIS topographies are based on outcomes of ice sheet modeling studies [*Robinson et al.*, 2011; *Born and Nisancioglu*, 2012]. EEMr1 uses a moderately retreated GrIS from *Robinson et al.* [2011] with ice-free regions in northwestern and central western Greenland. EEMr2 includes a strongly retreated GrIS scenario from *Robinson et al.* [2011], where northern Greenland is completely deglaciated. Furthermore, the EEMr2 GrIS has a South Dome which is separated from the North Dome. For EEMr3, we use the same GrIS mask as in EEMr2, but we artificially remove the remaining South Dome. Finally, EEMr4 uses the Eemian GrIS proposed by *Born and Nisancioglu* [2012], which is characterized by deglaciation in northeastern and central western Greenland whereas northwestern Greenland and the summit area remain unchanged.

Due to the scarcity of proxy archives close to the GrIS margins, knowledge of the actual Eemian GrIS topography is very limited. However, the chosen topographies here are all in line with the presence of Eemian ice in Greenland ice cores (see *Merz et al.* [2014] for details). According to the surface elevation estimated from the NEEM core (pNEEM elevation $\geq \sim$2400 m) [*NEEM community members*, 2013], the EEMr1 and EEMr4 topographies seem to be more likely than EEMr2 and EEMr3. Indeed, EEMr3 serves as an idealized simulation to estimate the role of the South Dome but is not a realistic Eemian melting scenario, as southern Greenland likely remained glaciated throughout the Eemian according to recent proxy evidence [*Willerslev et al.*, 2007; *Colville et al.*, 2011]. Note also that the implemented bed rock elevation of southern Greenland in EEMr3 is underestimated by several hundred meters with respect to present-day observations [*Bamber et al.*, 2013], implying that EEMr3 rather overestimates the effect of a complete deglaciation in southern Greenland.

As an important prerequisite, the model has to be evaluated against observational data to show its ability to reproduce the climatic processes under investigation. In this regard, *Merz et al.* [2013] previously showed that Greenland precipitation (and accumulation) is reasonably represented in CCSM4 for present-day climate conditions. Moreover, the model also realistically captures the relationship between a local Greenland precipitation event and the associated synoptic atmospheric circulation pattern. However, as the model shows a general overestimation in summer precipitation, some care must be taken when assessing seasonality issues. A detailed evaluation of Greenland's surface mass balance is also provided by *Vizcaino et al.* [2013], who used the fully coupled CCSM4 (denoted as CESM1 therein) and found that the model realistically simulates Greenland's hydrological cycle. In the framework of this study, we additionally evaluate the model's ability to simulate Greenland weather patterns and back trajectories (see sections 2.2 and 2.3) using ERA-Interim (ERAi) reanalysis data [*Dee et al.*, 2011] as observational reference.

Within this study we further focus on precipitation changes at the pNEEM site (indicated as red dot in all map plots, e.g., Figure 1). To account for surface heterogeneities in the model and for uncertainty in the true pNEEM position, we calculate the pNEEM values by averaging over the 3×3 grid points located closest to the suggested pNEEM site. pNEEM is located in the plateau area assuming a present-day configuration of the GrIS (EEMpd, Figure 1). In contrast, the strongly reduced scenarios in EEMr2 and EEMr3 lead to a major inland shift of the ice edge, changing the pNEEM conditions to the ones characteristic for the North Dome slope areas.

2.2. Weather Pattern Analysis

We use circulation-type classification based on the *k* means clustering algorithm [*Michelangeli et al.*, 1995] in order to define Greenland weather patterns that describe typical synoptic situations. The analysis of such weather patterns allows detailed insights into how the atmospheric circulation contributes to regional precipitation and to what extent this relationship can change [*Hofer et al.*, 2012]. The *k* means method agglomerates data around randomly chosen cluster seeds and iteratively finds the partition that minimizes the variance within the clusters [*Michelangeli et al.*, 1995]. To avoid a local optimum, the clustering is repeated 1000 times with randomly varied initial seed partitions. A stable solution is reached once the cluster seeds stop moving during the iterative process of minimizing the variance. Eventually, the algorithm provides a characteristic weather pattern for each of the final clusters, so-called centroid patterns.

We apply the *k* means algorithm to the 20 leading principle components (explaining >95% of the total variance) of daily mean 500 hPa geopotential height (*z*500) data covering the spatial domain of 50°N–90°N/110°E–30°W. This region is centered around Greenland but also includes substantial parts of the Canadian Archipelago, the North Atlantic, and northwestern Europe. The method is separately applied to daily winter (December-January-February (DJF)) and summer (June-July-August (JJA)) data to obtain independent seasonal weather patterns. The choice of the number of clusters *k* needs to be defined a priori and is therefore a critical quantity. To determine the optimal number of clusters, the algorithm is applied to ERAi data varying *k* from 2 to 15 and estimating the within-type variability and the separability of the respective weather patterns using different metrics, e.g., explained variation, within-type standard deviation, and pattern correlation ratio [*Huth et al.*, 2008, and references therein]. The results of the different metrics are diverse but show that during winter and summer at least four clusters are needed. Thus, our analysis was conducted with $k = 4$, 6, and 10 clusters but—as the main conclusions are very similar—only results for $k = 4$ are shown.

To assess the model's ability to simulate weather patterns, we compare the $k = 4$ weather patterns from ERAi reanalysis with the ones from PD simulation data. In particular, for the winter season, we find good agreement between the ERAi and PD weather patterns (Figures 2a and 2b). Thus, the model is capable of simulating the main weather situations over Greenland. In summer, when the atmospheric variability is generally less distinct, the model has some difficulties in simulating JJA pattern 1 found in ERAi (compare Figures 2c and 2d) whereas the other three PD weather patterns reasonably agree with the ones deduced from ERAi.

In order to assess the stability of the Greenland weather patterns during Eemian climate conditions, we compare the patterns obtained from the Eemian simulations with the ones from PI by calculating the spatial correlation and the projected frequencies of occurrence. For the latter, each of the 2700 winter days and 2760 summer days is assigned to one of the centroid patterns of the PI simulation by calculating the spatial correlation coefficients between the daily mean *z*500 pattern and all centroid patterns of the corresponding season. The day is then assigned to one of the four weather patterns with which it has its maximum spatial correlation. The relative frequency of occurrence of the PI weather patterns is the number of days associated with the respective pattern divided by the total number of days in the corresponding season. Besides the occurrence of the weather patterns, we further investigate the stability of the precipitation patterns associated with each of the weather patterns using a simple composite analysis. All days assigned to a certain weather pattern build the corresponding composite for which we calculate the mean precipitation pattern.

2.3. Back Trajectory Analysis

To gain insight into possible changes of the Eemian moisture transport toward the pNEEM site, three-dimensional trajectories are calculated using the Hybrid Single-Particle Lagrangian Integrated Trajectory (HYSPLIT) model provided by the National Oceanic and Atmospheric Administration Air Research Laboratory [*Draxler and Hess*, 1998]. All trajectories start at pNEEM (75.9°N/46.0°W), and the chosen setup uses an upper boundary height of 15 km and isentropically calculated vertical motions. All trajectories are run backward for 10 days (240 h), and three-dimensional coordinates (latitude, longitude, and height) are saved every hour along the trajectory. For each data set (ERAi and all simulations) we calculate a 30 year trajectory climatology, each of them containing 43,800 trajectories (the start interval is 6 h). Moreover, two different starting heights (500 m and 1500 m above ground level) are used. As the resulting climatologies of trajectories look very similar, only results which employ the starting point 1500 m above pNEEM are shown. Furthermore, the sensitivity of the trajectories to a slight horizontal shift of the starting position was tested,

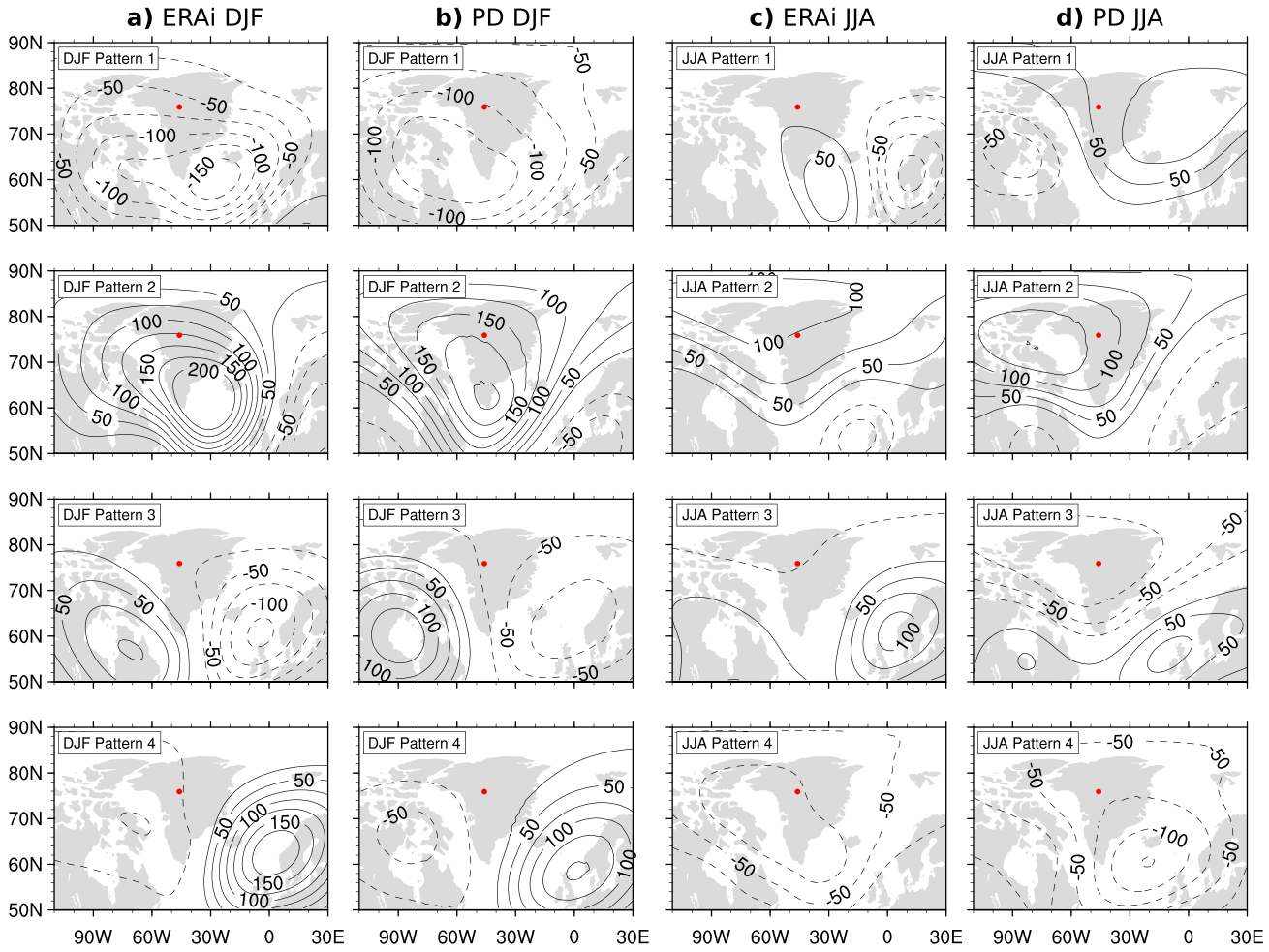

Figure 2. Greenland 500 hPa geopotential height (*z*500) centroid patterns determined by the *k* means (*k* = 4) cluster analysis applied to (a) ERAi winter (DJF), (b) PD winters, (c) ERAi summers (JJA), and (d) PD summers.

showing that single trajectories can vary considerably with a slight change in starting point. However, the climatologies of trajectories (i.e., larger ensembles of trajectories) demonstrate little dependence on slight horizontal shifts of the starting point.

As input data for HYSPLIT we use 6-hourly output from our simulations and ERAi which comprise surface fields (surface temperature and surface winds) as well as upper air fields, namely, the three-dimensional wind components, geopotential height, relative humidity, and temperature at 16 pressure levels ranging from 1000 to 100 hPa. The trajectories of the EEM simulations are calculated using the corresponding topography mask (shown in Figure 1) as invariant terrain height files.

To identify the trajectories that are relevant for the moisture transport toward pNEEM, we subsequently add a wet-day criterion. Hence, the sample of trajectories are restricted to start at days when precipitation at pNEEM exceeds 1 mm/day. As pNEEM is characterized by relatively dry conditions, this substantially reduces the sample size, e.g., for PI winters, only 660 of 10,800 trajectories fulfill the wet-day criterion (for PI summers, this statistic increases to 3624 of 11,200). As we aim for qualitative statements regarding the moisture transport to pNEEM, no further criteria are added (e.g., moisture uptake and evaporation en route [*Sodemann et al.*, 2008]). We rather focus on the short-term (24 h to 72 h) transport routes shortly before the precipitation event at pNEEM to depict from which adjacent areas (e.g., Labrador Sea or Baffin Bay) the responsible moist air parcels come.

In order to determine the skill of this back trajectory analysis, we evaluate the pNEEM wet-day 24 h back trajectories of the PD simulation with the trajectories found within ERAi (Figure 3). Generally, the model shows

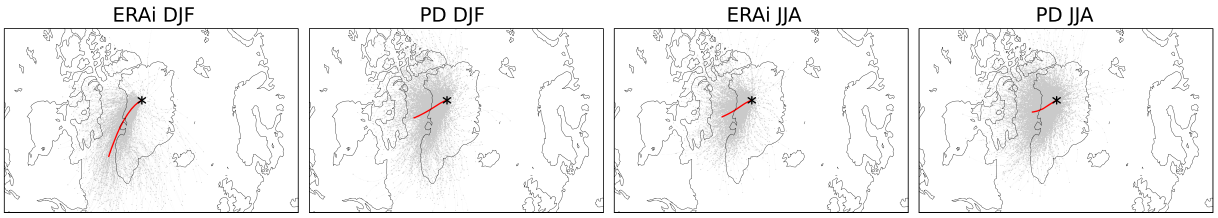

Figure 3. Ensembles of 24 h back trajectories prior to precipitation events at pNEEM in ERAi and the PD simulation for winter (DJF) and summer (JJA). The mean trajectory of the respective ensemble is indicated as red line.

reasonable capability in reproducing the winter and summer trajectory climatologies found for ERAi. This is true in terms of both the mean trajectory (red lines in Figure 3) and the range covered by all trajectories. In winter, the model exhibits a bias toward a too westerly flow compared to the ERAi trajectories. The PD summer climatology, on the other hand, matches ERAi very well.

3. Greenland Precipitation During Preindustrial Climate

Greenland's precipitation is characterized by a pronounced spatial pattern (shown for PI in Figure 4). The regional amount of precipitation is regulated by atmospheric conditions (water vapor content and circulation) combined with topography [*Ohmura and Reeh*, 1991; *Dethloff et al.*, 2002]. Greenland's mean precipitation pattern is characterized by two general tendencies: First, precipitation decreases from south to north as, on the one hand, southern Greenland is exposed to the North Atlantic storm track, which frequently brings a lot of moisture, and on the other hand, the very cold temperatures in the Arctic result in a severe lack of moisture in northern Greenland. Second, coastal areas receive more precipitation than inland regions as precipitation is mostly deposited during orographic lifting over the steep slopes of the GrIS.

Moreover, the Greenland precipitation pattern clearly depends on the respective season. In winter (Figure 4a), most precipitation falls over the slopes in southern and eastern Greenland. Westerly flow crossing the southern tip of Greenland induces lee cyclogenesis, strengthening the Icelandic low [*Chen et al.*, 1997; *Kristjansson and McInnes*, 1999]. The Icelandic low itself causes strong easterly onshore winds resulting in the winter precipitation maximum in southeastern Greenland [*Schuenemann et al.*, 2009]. A secondary winter cyclone maximum is found in Baffin Bay [*Tsukernik et al.*, 2007] as the cyclones approaching Greenland from the southwest can also travel along Greenland's west coast [*Chen et al.*, 1997]. However, winter precipitation in western Greenland is clearly less frequent. In summer, the atmospheric circulation is weaker, and synoptic systems generally approach Greenland from the west. Consequently, the dominant synoptic forcing of Greenland summer precipitation is associated with (weak) cyclones in Baffin Bay [*Schuenemann et al.*, 2009], and as a result, western Greenland receives substantial summer precipitation, exceeding precipitation in eastern Greenland (Figure 4b).

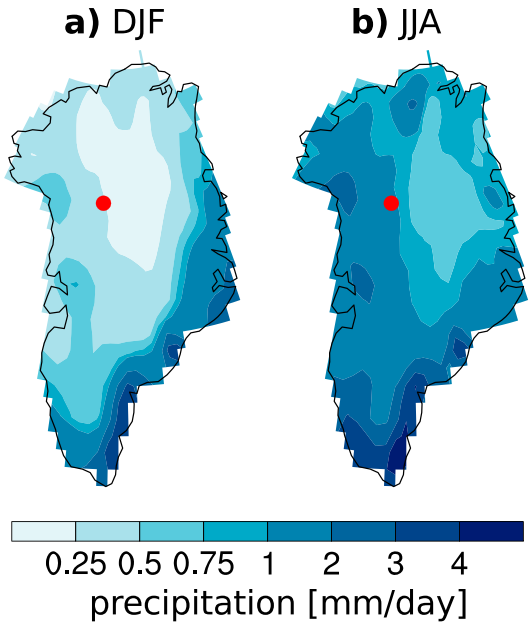

Figure 4. Mean precipitation (mm/day) for (a) winter (DJF) and (b) summer (JJA) over Greenland in the PI simulation.

4. Greenland Precipitation During the Eemian

4.1. Effect of Orbital Forcing

Compared to preindustrial conditions, the Northern Hemisphere (NH) Eemian climate is dominated by the orbital forcing, with a substantial increase of the solar insolation seasonality, particularly in the NH high latitudes. The response of the hydrological cycle to this forcing is closely tied to concurrent changes in the temperature field. Comparing Greenland

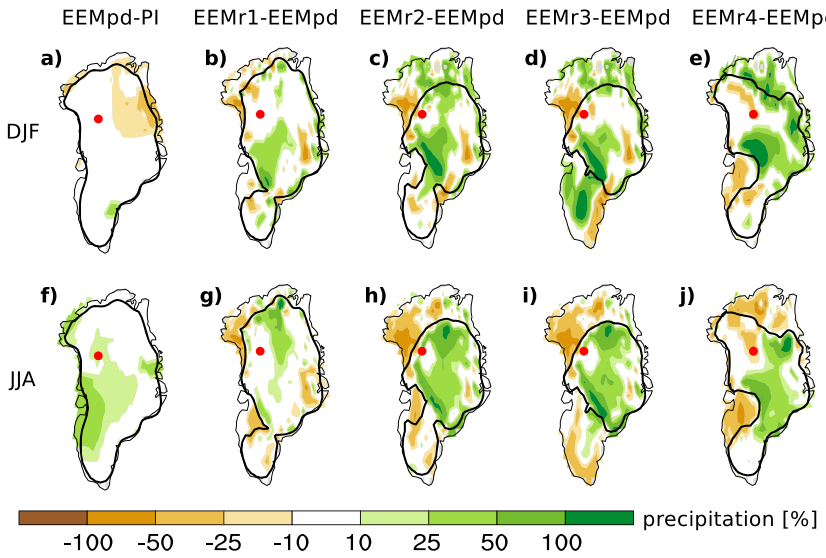

Figure 5. Precipitation differences (relative changes in %) due to orbital forcing and changes in the GrIS topography for (a–e) winter (DJF) and (f–j) summer (JJA), respectively. Note that only significant precipitation changes are drawn (using 5% significance level and *t* test statistics). The black contour lines indicate the edges of the corresponding GrIS.

surface air temperatures (SAT) of EEMpd with PI, we find an insolation-driven summer warming of 2–4°C [*Merz et al.*, 2014], in agreement with results from other climate models [*Lunt et al.*, 2013; *Nikolova et al.*, 2013] and proxy data [*CAPE Last Interglacial Project Members*, 2006]. In contrast, Greenland temperatures are marginally affected by the Eemian reduction in winter insolation, because the solar insolation is by definition largely absent at high latitudes during this season. The simulated EEMpd DJF temperatures over Greenland are therefore moderately colder but not significantly different from PI [*Merz et al.*, 2014]. The NH large-scale atmospheric circulation in EEMpd exhibits only moderate changes compared to PI and the general flow characteristics, i.e., a strong Icelandic low in winter and the westerly flow in summer remain [*Merz et al.*, 2014]. Consequently, Greenland precipitation changes due to the orbital forcing are expected to depend on changes in the moisture source rather than modifications in the transport and deposition (controlled by the atmospheric flow) of moisture.

The simulated EEMpd-PI response in Greenland precipitation is shown in Figures 5a and 5f. Generally, the orbitally forced precipitation anomalies over Greenland are moderate in contrast to much larger changes in the hydrological cycle at lower latitudes found by *Nikolova et al.* [2013]. In winter (Figure 5a), the only significant change in precipitation is a drying of the northeastern part of Greenland. This reduction is related to a positive sea ice anomaly along Greenland's east coast (not shown). As winter precipitation in northeastern Greenland is found to be largely associated with easterly flow (discussed in detail in section 4), this enlarged sea ice cover limits evaporation, lowering the region's moisture availability and eventually decreasing precipitation in northeastern Greenland.

In summer (Figure 5f), the orbital forcing leads to enhanced precipitation in the western half of Greenland. Like the EEMpd-PI winter anomaly, this summer increase is related to changes in the moisture availability rather than to changes in the moisture transport to Greenland. In fact, we find that for EEMpd the atmospheric circulation rather exhibits a weakening of the westerly circulation [*Merz et al.*, 2014], which (if dominant) would imply a drying of western Greenland. However, the NH summer temperatures lead to an enhanced hydrological cycle and cause significantly stronger evaporation in the regions upstream of Greenland, namely, northeastern America and the Canadian Arctic Archipelago (not shown). The additional moisture is then transported with the westerly flow to Greenland where it mainly precipitates over the western slopes. Averaged over the entire GrIS, annual mean precipitation thus slightly increases from 390 to 405 mm/yr due to the Eemian orbital forcing as the small decrease in winter is overcompensated by the enhanced hydrological cycle during the Eemian summer climate. The higher summer temperatures further lead to an increase of summer precipitation falling as rain instead of snow.

4.2. Effect of Reduced GrIS Topography

As seen for preindustrial conditions (Figure 4), the regional distribution of precipitation is clearly shaped by the ice sheet topography. Thus, we expect significant changes of the precipitation pattern in the Eemian simulations with a reduced GrIS compared to EEMpd. Indeed, the local changes in precipitation due to changes in the ice sheet topography are larger than the precipitation changes associated with the orbital forcing (Figure 5). The precipitation change patterns are quite complex and include many small-scale features associated with the local topography. This emphasizes the importance of the actual GrIS shape on Greenland's precipitation distribution. The general tendency is that newly ice free areas become drier whereas the precipitation on the remaining ice sheet increases. This seems intuitive as Greenland's precipitation is strongly bound to orographic lifting, and as the slopes of the ice sheet move inland the major precipitation areas seem to move with them. However, in winter we also observe wetter conditions in deglaciated areas in northeastern Greenland (Figures 5c–5e). This is likely explained by the fact that a reduction in GrIS size and height weakens the barrier effect of the ice sheet, allowing cyclonic systems to penetrate into more central and northern regions of Greenland. These simulated effects are in agreement with the findings by *Hakuba et al.* [2012], who found that presently dry regions receive enhanced precipitation and wet regions become drier in their idealized simulations in which flatter GrIS topographies were incorporated.

In addition to many consistent features, the detailed comparison of the winter and summer precipitation responses (Figure 5) reveals some precipitation changes that vary substantially between the two seasons. For instance, northeastern Greenland experiences a wetter winter but drier summers in the experiments where the region becomes ice free (e.g., EEMr4). As another example, the removal of the South Dome in EEMr3 leads to a westward shift in South Greenland's winter precipitation, whereas in summer the response shows a general decrease in precipitation along the coasts coinciding with enhanced precipitation in inland regions. The seasonal variations are related to the fact that winter circulation is clearly distinguished from that in summer, and each season therefore features specific flow characteristics of the moist air masses moving toward Greenland. The atmospheric circulation in winter is dominated by the strong Icelandic low, while in summer the circulation is predominantly westerly. Thus, it is not surprising that the reduced Eemian GrIS topography exhibits a seasonally different imprint on the precipitation pattern of Greenland.

Interestingly, Greenland's average precipitation remains relatively constant throughout all Eemian simulations (approximately 400 mm/yr). This demonstrates that modifications in the GrIS topography just lead to a redistribution of the available moisture but do not change Greenland's total moisture budget. This is unexpected as we observe a strong increase in summer evaporation in the simulations with a small GrIS (not shown), mostly where large ice-free areas are exposed to the relatively warm Eemian summer climate. However, the increase in evaporation (from 30 to 50 mm/yr averaged over the GrIS) does not result in a concurrent increase in Greenland's total precipitation. Hence, the evaporated moisture is not recycled above the remaining ice sheet but rather transported away by the atmospheric flow. The widespread lowering of Greenland's surface elevation in the EEMr1-EEMr4 simulations and the associated surface warming further increases the fraction of summer precipitation falling as rain rather than snow. While in the PI experiment the model simulates 25% of Greenland's summer precipitation as rain, this fraction increases to about 40% in EEMpd and to almost 60% in EEMr3. In contrast, all winter precipitation falls as snow regardless of the choice of the GrIS.

In summary, considerable melting of the Eemian GrIS is found to have a distinct impact on the local precipitation field. However, no related changes are identified in more distant regions as the response of the NH precipitation pattern is mostly negligible in the periphery of Greenland even for the strongest GrIS retreat scenario (EEMr3; shown for DJF in Figure 6b). This is in contrast to the effect of the Eemian orbital forcing causing hemispheric-scale precipitation changes (not shown). In fact, a significant effect of a reduced GrIS on distant regions would require changes in the large-scale circulation. However, as previously discussed in *Merz et al.* [2014], the mean large-scale circulation remains very stable among all Eemian simulations. This is confirmed by the analysis of the NH winter storm track (Figure 6), which shows that even in EEMr3 there are only few significant changes in storm track activity. The most prominent anomaly in EEMr3 is an increase in eddy activity southwest of Greenland, which likely contributes to the precipitation increase in southwestern Greenland (Figure 6b). Consequently, changes in Greenland's topography during the Eemian appear to exert a strong local forcing but are of minor importance for the Eemian climate on larger spatial scales.

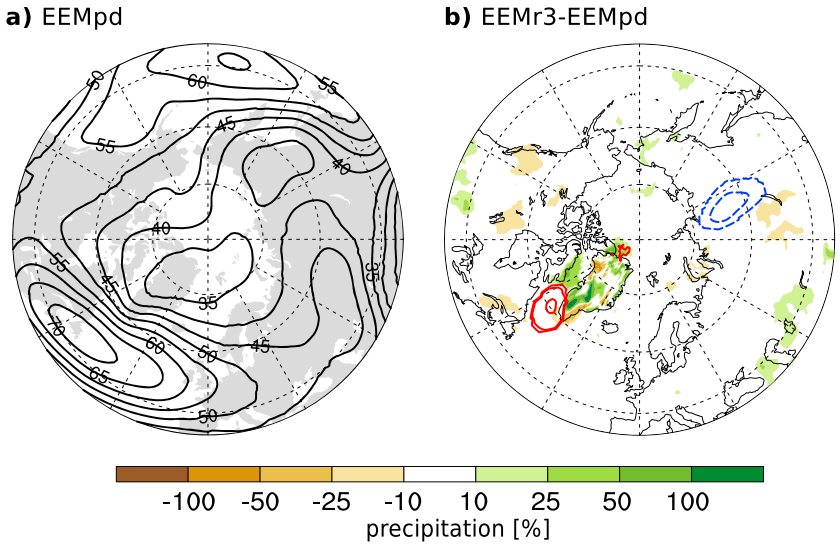

Figure 6. (a) EEMpd climatological winter storm track (defined as standard deviation of 2.5–6 day band pass-filtered 500 hPa geopotential height). (b) EEMr3-EEMpd anomalous precipitation (shaded; relative changes in %) and changes in storm track activity (contours; gpm). Contour interval is 2 gpm with positive (negative) anomalies denoted in red (blue) color. Note that in Figure 6b only significant anomalies are drawn (using 5% significance level and *t* test statistics).

5. Role of Greenland Weather Patterns

In order to investigate the relationship of the simulated precipitation anomalies to specific atmospheric flow patterns in detail, we apply the cluster analysis that classifies the daily weather situations into a number of so-called Greenland weather patterns (details given in section 2.2).

5.1. Winter Patterns

The four DJF patterns are shown in Figure 7a. Pattern 1 is characterized by anomalous low-pressure south of Greenland resulting in southeasterly flow toward the ice sheet. Consequently, this weather pattern brings moist air masses from the North Atlantic to eastern Greenland where (in the presence of the present-day GrIS) it precipitates over the steep coastal areas as shown by the corresponding precipitation composite (Figure 7c). Pattern 2 exhibits anomalous anticyclonic activity centered above the Labrador Sea leading to northwesterly flow toward Greenland. Due to their continental source, these air masses are rather dry, and the associated precipitation composite indeed shows limited precipitation over Greenland. If precipitation occurs in this weather situation, it falls along the western coast of Greenland. Pattern 3 includes anticyclonic flow around Hudson Bay, resulting in anomalous northwesterly flow toward western Greenland. Similar to pattern 2, these continental air masses are very cold and dry and, thus, rarely lead to precipitation. However, in contrast to pattern 2, the anticyclonic anomaly ("blocking") does not affect eastern Greenland; hence, precipitation is observed in southeastern Greenland related to onshore flow due to the Icelandic low. Lastly, pattern 4 can be regarded as the counterpart to pattern 3, where a southerly flow of relatively warm and moist air moves toward Greenland and brings substantial winter precipitation to southern Greenland, leaving the northern part mostly dry.

The four characteristic winter weather patterns (Figure 7a) identified for present-day/preindustrial climate are found in all Eemian simulations as well. Hence, the Eemian orbital forcing as well as the tested changes in GrIS topography do not change the large-scale structures of these weather patterns. Comparing the relative frequencies of the patterns in the respective simulations (indicated by the red bars in Figure 7b), we additionally observe that their temporal occurrence remains fairly stable in all simulations. Pattern 1 is the leading pattern occurring at around 35–40% of all winter days, followed by pattern 4 (25%), pattern 3 (20%), and pattern 2 (15%).

Consequently, the precipitation changes due to altered ice sheet topography are not explained by the anomalous occurrence of specific weather patterns. Nevertheless, we find distinct differences between the precipitation composites calculated for the Eemian simulations with a reduced GrIS (Figures 7d–7g)

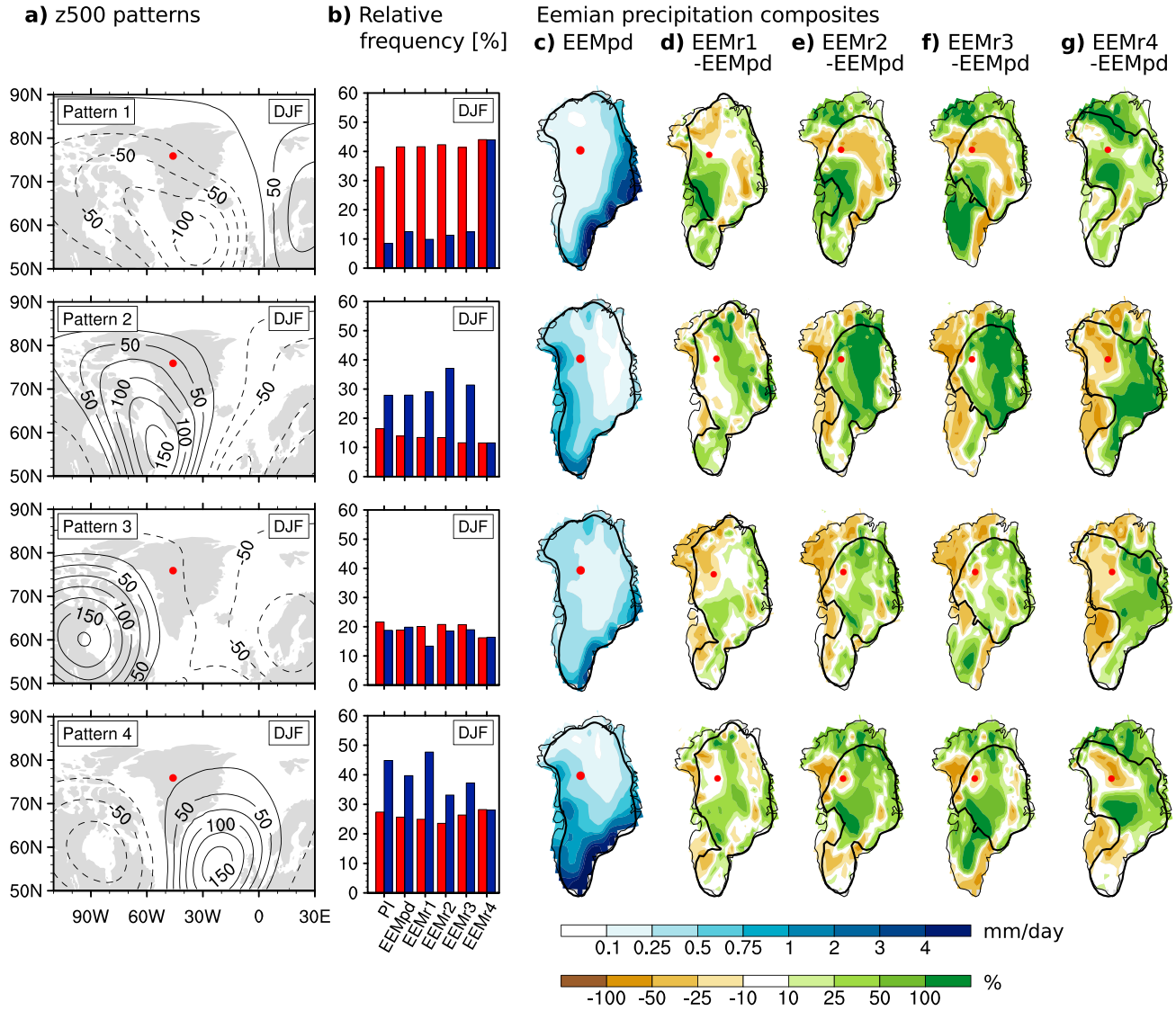

Figure 7. Winter (DJF) Greenland weather patterns and the corresponding precipitation patterns. (a) PI weather patterns shown as 500 hPa geopotential height anomalies (m) from the DJF mean. (b) The red bars show the relative frequencies (in %) of the projected weather patterns shown in Figure 7a in the PI and EEM simulations. The relative frequencies (in %) of the projected weather pattern during precipitation events at pNEEM are shown by the blue bars. (c) The EEMpd absolute precipitation composite (mm/day) corresponding to each weather pattern. (d–g) EEMr1-EEMr4 precipitation composites shown as differences (relative changes in %) from the EEMpd composite shown in Figure 7c.

compared to the EEMpd composites (Figure 7c). Thus, the topography controls in which areas moist air masses are lifted and cause orographic precipitation. For example, the easterly flow associated with pattern 1 brings significantly more precipitation to regions in western Greenland in the EEM experiments including a retreated GrIS. This is related to a reduction of the barrier effect (compared with EEMpd; Figure 7c), which blocks moist air masses from moving past the upwind slope. As a result, pattern 1 causes less precipitation over eastern Greenland in EEMr1-EEMr3 as the smaller GrIS makes it easier for the wet air masses to flow around the ice sheet and precipitate elsewhere. Equivalent effects on the upwind side (precipitation decrease) and in regions located more inland or leeward (enhanced precipitation) are also observed for weather patterns 2–4.

5.2. Summer Patterns

The four Greenland weather patterns derived from JJA data are shown in Figure 8a. Compared to the winter patterns described above, the summer weather patterns are less pronounced as the NH summer circulation is generally less variable than the winter circulation. The four summer clusters comprise anomalous

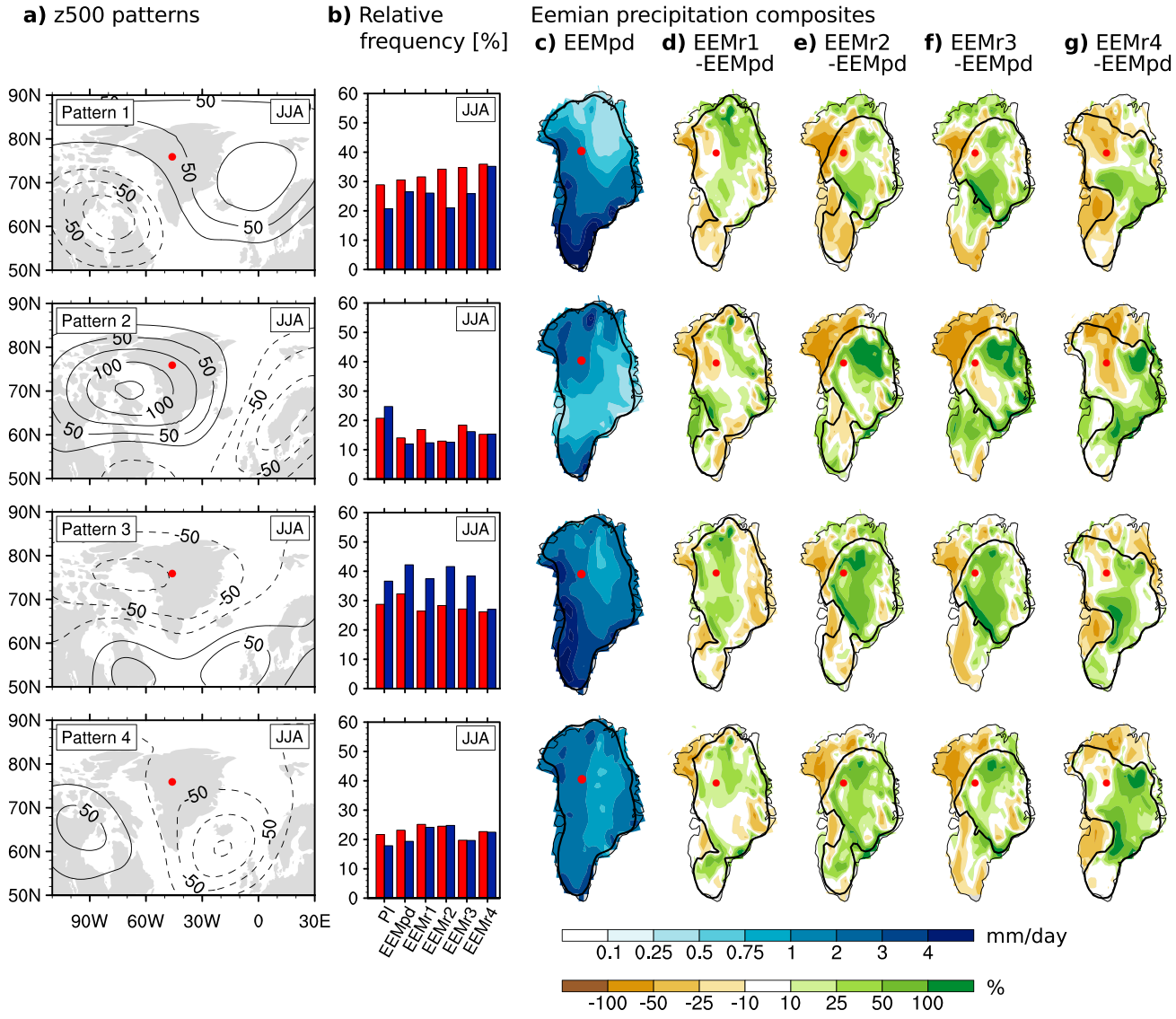

Figure 8. Same as Figure 7 but for summer (JJA).

southerly (JJA pattern 1), northwesterly (JJA pattern 2), westerly (JJA pattern 3), and northeasterly (JJA pattern 4) flows. Due to the warmer temperatures, the NH summer air masses contain more moisture, so all four summer patterns are able to generate substantial precipitation over Greenland (Figure 8c).

As in winter, the projection of the PI summer patterns on the EEM simulations shows that their frequencies are fairly constant across all simulations (Figure 8b). More precisely, patterns 1 and 3 are the leading synoptic situations, each occurring during approximately 30% of all summer days, independent of the orbital forcing (Eemian or PI) and the implemented Eemian GrIS topography. On the other hand, pattern 4 (20%) and pattern 2 (around 15%) are less frequent in all model experiments. Hence, the atmospheric circulation above Greenland is again found to be rather stable for all Eemian simulations. Consequently, the precipitation differences in summer (Figure 5b), as in winter, are linked to changes in the position of the Greenland slopes where the moist air masses are exposed to lifting. This is confirmed by the summer precipitation composites (Figures 8d–8g), which are clearly shaped by the GrIS topography and hence very different in the perturbed EEM simulations than in EEMpd.

Thus, the same two concepts apply as in winter: first, deglaciated but previous slope areas, which are exposed to moist air masses, i.e., lying on the upwind side during the respective weather pattern, are characterized by a substantial drying. At the same time, regions located closer to the ice sheet margin compared

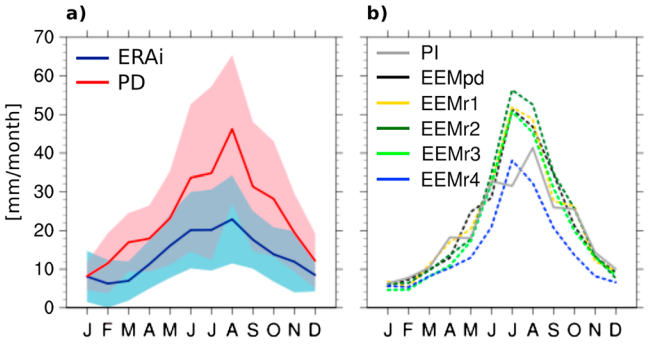

Figure 9. Seasonal cycle of precipitation at pNEEM (mm/month). (a) Comparison of PD with ERAi including the monthly standard deviation (shaded). (b) Comparison of the PI and Eemian simulations.

to EEMpd receive enhanced precipitation. Second, regions that lie leeward during a specific weather pattern receive more precipitation in the simulations, including a smaller GrIS due to the reduced barrier effect. For example, eastern Greenland remains dry in EEMpd during JJA pattern 2 as it is located on the downwind side but receives significantly more precipitation in EEMr4 when the moist air masses can flow around the reduced ice sheet (Figure 8g).

Within the framework of these weather patterns, we are able to understand the seasonally dependent response in Greenland's precipitation to the tested changes in the GrIS topography (as described in section 4.2). In winter, precipitation over Greenland is predominantly associated with southerly and easterly flow (winter weather patterns 1 and 4 in Figure 7), so western and northern Greenland experience the lee effect. In the experiments where the GrIS is reduced, these leeward areas become wetter. In summer, all four weather patterns are connected to substantial precipitation (Figure 8c). Hence, though the summer circulation is predominantly westerly, moisture can be advected from all directions and there are no regions that are dominantly upwind or leeward. We rather observe the "moving slope effect," i.e., summer precipitation increases over the new slopes and inland areas, whereas precipitation declines over the flatter, ice-free areas outside of the ice sheet.

6. Eemian Precipitation at pNEEM

6.1. Precipitation Seasonality

At present, pNEEM is characterized by dry conditions as it is located high on the GrIS, far from the slope areas where moist air masses are orographically lifted and subsequently condense and precipitate. Moreover, the limited amount of precipitation at pNEEM undergoes a distinct seasonal cycle with the majority of moisture deposited during the summer months (Figure 9). The comparison of the PD simulation with ERAi (Figure 9a) reveals that the model clearly overestimates summer precipitation at pNEEM; consequently, the simulated precipitation seasonality for present-day climate is too strong. The model's overestimation of summer precipitation is not specific for pNEEM but rather represents a large-scale model bias affecting the entirety of Greenland (not shown). Nevertheless, the spatial structure in Greenland precipitation/accumulation and the relationship of the atmospheric circulation causing summer precipitation in western Greenland conforms well with ERAi [*Merz et al.*, 2013]. The analysis of precipitation seasonality at pNEEM further reveals that interannual variability has a considerable amplitude during all months (shown as the monthly standard deviation in Figure 9a). This is observed for both ERAi and PD data. While the PD precipitation variability exceeds ERAi in absolute terms, the relative standard deviation is on the order of 50% of the monthly mean precipitation in both cases.

Comparing pNEEM precipitation simulated for EEMpd with PI, we find that the Eemian orbital forcing leads to a significant increase of pNEEM summer precipitation (Figure 9b). In contrast, EEMpd winter precipitation remains at low levels, and thus, the seasonality of precipitation at pNEEM is strengthened for Eemian climate conditions. Alteration of the GrIS topographies can have an effect on pNEEM's precipitation as well. EEMr1, EEMr2, and EEMr3 only weakly deviate from the EEMpd annual cycle in precipitation (Figure 9b). In contrast, the EEMr4 topography leads to an all-year precipitation reduction compared to EEMpd. This precipitation decrease (in absolute terms) is strongest during the summer months. The dynamical cause for this precipitation decline can be identified using the weather pattern analysis. For all winter and summer weather situations (except DJF pattern 1) the EEMr4 topography leads to anomalous precipitation in eastern Greenland at the expense of northwestern Greenland including pNEEM (Figures 7g and 8g).

6.2. Moisture Transport Toward pNEEM

In order to investigate the dynamical origin of pNEEM's precipitation, we calculate the relative frequencies of the weather patterns occurring during wet days at pNEEM, i.e., during days when the precipitation exceeds

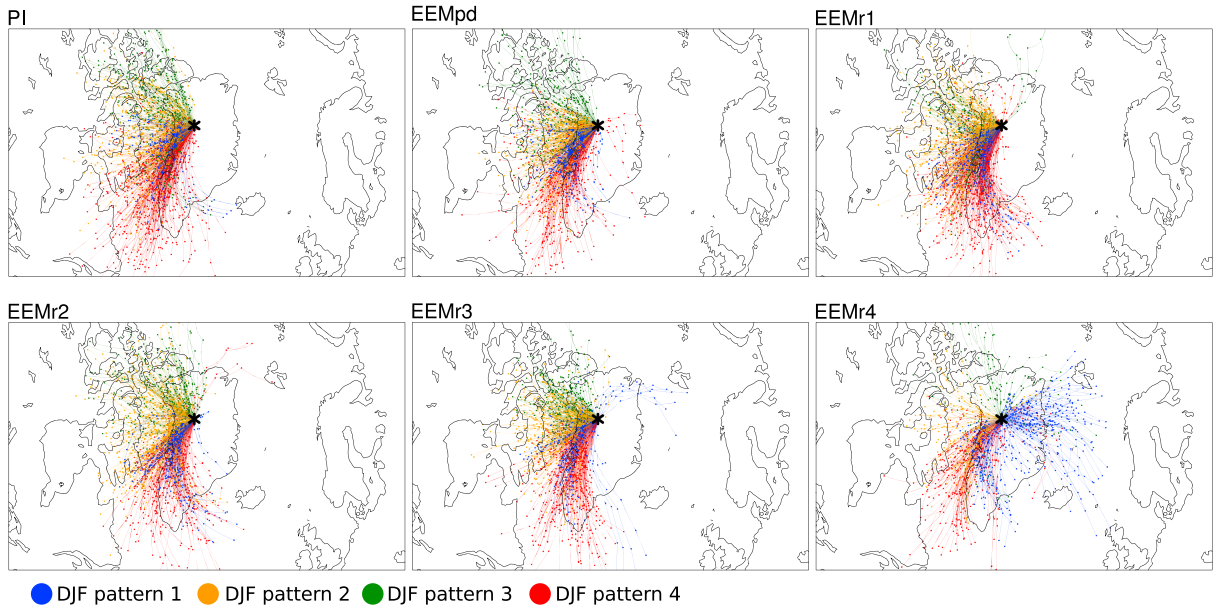

Figure 10. Ensemble of 24 h back trajectories prior to winter (DJF) precipitation events at pNEEM in PI and all Eemian simulations. The trajectories are clustered according to the cooccurring DJF weather patterns.

1 mm/day. The results for the respective simulations are indicated by the blue bars in Figure 7b for winter and in Figure 8b for summer months. As a second measure for the moisture transport toward pNEEM, we determine the transport routes of the air parcels prior to pNEEM wet days with the aid of the Lagrangian back trajectory analysis (section 2.3 and Figures 10 and 11). For the purpose of comparison, the trajectories are clustered according to the cooccurring seasonal weather patterns.

For PI winters we find that pNEEM precipitation events are mostly connected with anomalous southerly circulation as DJF pattern 4 (Figure 7a) occurs during 45% of pNEEM's winter wet days (Figure 7b). Furthermore, DJF pattern 2 (large-scale westerly flow) accounts for another 30% of pNEEM's wet days. The corresponding 24 h back trajectories for PI winter wet days (Figure 10a) confirm that moisture is predominantly advected from western and southern directions. In fact, almost all PI winter trajectories originate west of pNEEM

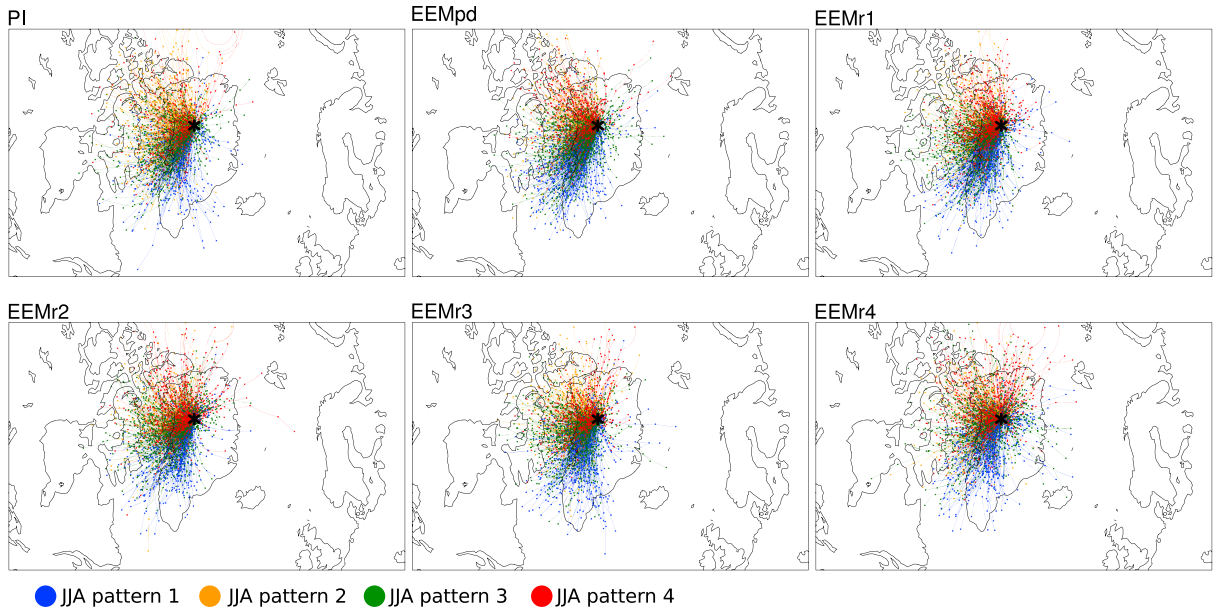

Figure 11. Same as Figure 10 but for summer (JJA).

irrespective of the cooccurring weather pattern, and in neither case is moisture advected from east of the GrIS, i.e., from the Norwegian Sea. This is in agreement with the fact that large-scale easterly flow toward Greenland (captured by the DJF pattern 1, Figure 7a) rarely results in precipitation at pNEEM, as indicated by the very low relative frequency of pattern 1 during pNEEM wet days (see blue bars in Figure 7b). Consequently, the present-day GrIS acts as a perfect barrier and prevents any moist air originating from the east from arriving at pNEEM.

In the Eemian simulation (except for EEMr4), the weather pattern analysis shows that DJF patterns 2 and 4 are the dominant weather situations causing precipitation at pNEEM as previously observed for PI climate (Figure 7b). At the same time, the relative importance of these two patterns is subject to slight variations (most distinct for EEMr2). Nevertheless, we find that neither the Eemian orbital forcing nor the relative shift of pNEEM closer to the ice sheet edge (e.g., in EEMr2 and EEMr3) results in a change of pNEEM's moisture source characteristics. These findings are supported by the winter back trajectories (Figure 10), which show that for all simulations except EEMr4 the moist air masses come from western directions (ranging from northwest to south) whereas the easterly direction is completely blocked by the GrIS, which acts as a topographic barrier. Additionally, a few trajectories starting southeast of Greenland make their way up to pNEEM by flowing around the North Dome. In contrast, a fundamental change in pNEEM's moisture transport is found in the EEMr4 simulation as is obvious from both analyses: according to the DJF weather pattern analysis, pattern 1 (easterly flow) becomes the dominant weather situation in EEMr4 causing precipitation at pNEEM, whereas the occurrence of pattern 2 during pNEEM wet days is highly decreased (Figure 7b). While the large-scale easterly flow usually causes (i.e., in all other simulations) precipitation over the slopes of eastern Greenland (see precipitation composite for pattern 1 in Figure 7c), the EEMr4 GrIS topography allows the moist air masses to travel to northwestern Greenland and to precipitate there. In agreement with this, the ensemble of EEMr4 back trajectories (Figure 10) exhibits additional trajectories transporting moisture from the Norwegian Sea to pNEEM.

The EEMr4 GrIS topography (Figure 1), where pNEEM is exposed to the northeastern ice sheet margin, thus allows moisture advection from the east, in contrast to all other simulations. However, despite the fact that this easterly flow is a new moisture source, the total winter precipitation in EEMr4 is lower compared to the other Eemian simulations (Figure 9). This can be explained by the fact that the other three winter weather patterns bring substantially less moisture to pNEEM compared to EEMpd as is clear from the EEMr4 precipitation composites (Figure 7g).

As shown in section 4, the weather patterns in summer are less pronounced than in winter. As a consequence the four groups of pNEEM summer trajectories (Figure 11) as defined by JJA weather patterns cannot easily be distinguished. This is in clear contrast to the winter trajectories (Figure 10), where (except for the rare DJF pattern 1) the clustering of the 24 h back trajectories according to the four large-scale winter weather patterns gives very distinct results. The weaker summer circulation variability leads to the result that all four JJA patterns can lead to substantial precipitation at pNEEM as indicated by the precipitation composites (Figure 8c). However, calculating the frequencies of occurrence for PI pNEEM wet days, we find that pNEEM precipitation is primarily associated with the westerly circulation described by JJA pattern 3 (see blue bars in Figure 8b). The summer trajectories (Figure 11) support these findings, showing that moisture transport toward pNEEM is predominantly westerly. Similar to winter, there are only a few trajectories indicating moisture advection from the east; however, the barrier effect of the GrIS for wet air masses coming from the east is not as distinct as in winter.

Assessing the summer moisture transport in the Eemian simulations, we find that the relative frequencies of the JJA weather patterns during pNEEM precipitation events are relatively stable (Figure 8b) with some minor exceptions (e.g., pattern 2 in each Eemian simulation accounts for around 15% compared to 25% for PI). According to the weather pattern analysis, moisture transport to pNEEM is primarily westerly to southerly (JJA patterns 1 and 3) regardless of the GrIS topography. This is in agreement with the back trajectory analysis, which shows that all ensembles of JJA trajectories (Figure 11) are predominantly westerly prior to pNEEM precipitation events. The EEMr4 simulation displays some more trajectories originating over the Norwegian Sea, but compared to winter, these differences are of minor importance, and overall the summer moisture transport in all Eemian simulations looks very similar to PI conditions.

The back trajectory analyses for the spring and autumn seasons reveal a similar result as for winter. Hence, for PI and all Eemian simulations (except EEMr4) we find that moisture transport is predominantly

westerly, whereas moist air masses approaching from the east are always blocked by the GrIS and do not reach pNEEM (not shown). In contrast, the EEMr4 simulation allows additional moisture transport associated with easterly flow from the Norwegian Sea.

7. Relevance for Interpretation of NEEM Ice Core Proxies

Based on the presented results regarding changes and stability of Greenland's hydrological cycle and atmospheric circulation during the Eemian, we can provide insights into the interpretation of Eemian Greenland proxy records derived from the NEEM ice core.

The combination of snowfall and snow evaporation results in the accumulation signal, which is a key ice core quantity. The simulated annual mean accumulation (in millimeter liquid water equivalent per year) at pNEEM is 209 (PI), 225 (EEMpd), 237 (EEMr1), 217 (EEMr2), 174 (EEMr3), and 158 (EEMr4). Thereby, accumulation is dominated by precipitation, as pNEEM's location high on the GrIS prevents surface evaporation (at least in PI, EEMr1, and EEMr2). As shown in Figure 9b the Eemian orbital forcing leads to enhanced summer precipitation explaining the slight increase in EEMpd accumulation compared to PI. In addition, changes in topography can result in increased or decreased annual mean accumulation. In EEMr3 and EEMr4 the accumulation is clearly reduced compared to PI as in both cases the changed GrIS topography leads to a local decrease in snowfall. In EEMr3 a further decrease in accumulation results from strengthened snow evaporation as the pNEEM surface elevation is substantially lower and thus significantly warmer. Hence, the Eemian accumulation measured in the NEEM core is likely to vary during the last interglacial on millennial time scales as the GrIS topography changes during this period. Moreover, as EEMr4 exhibits the lowest accumulation at pNEEM followed by EEMr3 this provides evidence that the amount of the accumulation is not only linked to the size of the GrIS or pNEEM's elevation. Rather, this confirms the result that the actual shape of the GrIS is the key factor driving the local quantities of the hydrological cycle. Furthermore, it is important to note that the Eemian precipitation and accumulation changes found at pNEEM are hardly representative for larger Greenland areas due to the very local characteristics of the precipitation changes. This is particularly true for the precipitation response to changes in the GrIS topography.

For different aerosol species (e.g., sea salt and mineral dust) it is further important to know whether changes in the measured concentration and composition are related to source or transport processes. While source effects can not be analyzed within this study, we investigate the transport routes toward pNEEM with the aid of the back trajectory analysis. Transport prior to wet deposition is dominantly westerly to southerly during both preindustrial and Eemian climate conditions (see section 6.2). In contrast, advection of moist air masses from eastern directions is prohibited as long as pNEEM is located in the lee of the GrIS, which acts as a barrier. However, if the Eemian GrIS topography was at some point in time similar to the realization used in EEMr4 with pNEEM located more closely to the northeastern ice sheet margin, transport prior to wet deposition could also has been from the east. This additional group of easterly trajectories is found for autumn, winter, and spring, whereas the effect is less pronounced in summer. Thus, at least for aerosols predominantly deposited during the colder seasons, the EEMr4-like topography gives access to new source regions, which are presently beyond the area of influence for the NEEM ice core. Besides, the anomalous easterly advection of moisture in EEMr4 is expected to show up in the deuterium excess (another proxy for moisture source) found in the Eemian NEEM ice.

In contrast to wet deposition at pNEEM, which is limited to the relatively low number of precipitation days, dry deposition occurs rather constantly throughout the year. We analyzed the pNEEM back trajectory climatologies for a range of 1 to 10 days taking only dry days into account. The resulting trajectories cover large parts of the NH with an average transport from the southwest (not shown). This is in agreement with the trajectory climatology by *Kahl et al.* [1997], who assessed the transport routes to the summit region. Both the mean and the range of the dry day trajectory ensembles are rather constant throughout all simulations (not shown) implying that this climatological transport is largely independent of the Eemian orbital forcing and changes in the GrIS topography. Accordingly, we do not expect differing signals between the Eemian and the preindustrial dry-deposited aerosol concentrations related to changes in the transport routes.

8. Summary and Conclusions

In the course of this study, Greenland precipitation during the Eemian interglacial period was investigated using a set of CCSM4 simulations. In the process, we distinguish the sensitivity of precipitation to the Eemian

orbital forcing from the response to a reduction in the Greenland ice sheet (GrIS) volume. Greenland precipitation changes due to the orbital forcing are moderate (but significant) and generally driven by moisture availability, e.g., Greenland precipitation increases during the warm Eemian summers, as strengthened evaporation over upstream areas (North America) leads to additional moisture loading of the air masses eventually advected to Greenland. Modifications in the GrIS topography lead to very distinct precipitation changes, which reveal a very local signature emphasizing the fact that the actual shape of the GrIS is very important for Greenland's precipitation pattern. The moisture availability is rather constant among all Eemian simulations, but the GrIS topography determines in which areas the moist air masses are lifted and cause substantial precipitation. In agreement with *Hakuba et al.* [2012], we find that a flatter ice sheet weakens the barrier effect of the GrIS, thus allowing more moisture to be advected to the plateau and leeward areas. In contrast, precipitation is strongly decreased over Greenland areas that become flat and ice free.

Moreover, precipitation changes are seasonally different, as they are influenced by the atmospheric circulation transporting moist air masses toward Greenland that itself has a pronounced seasonality. With the aid of weather pattern analysis we demonstrate that winter precipitation is predominantly associated with southerly and easterly flow situation causing western and northern Greenland to experience the lee effect, i.e., increased precipitation in the experiments in which the GrIS size is reduced and the barrier effect of the GrIS is weakened. In contrast, during summer moisture can be advected from all directions so precipitation generally increases over the remaining GrIS and decreases in deglaciated regions. The occurrence of daily weather patterns is stable in all Eemian simulations and therefore not significantly affected by a substantial reduction of the Eemian GrIS. Hence, the topography-related precipitation changes are not driven by variations in the occurrence of specific weather situations but rather by changes in the precipitation signature of the respective weather patterns.

The implemented reductions in GrIS topography do not result in significant large-scale responses; i.e., precipitation changes outside of Greenland are negligible. This is related to the absence of significant changes in the NH large-scale circulation as previously shown in *Merz et al.* [2014]. These results are somewhat unexpected in light of the fact that previous "No-Greenland" experiments showed significant changes in NH circulation and storm track statistics [*Petersen et al.*, 2004; *Dethloff et al.*, 2004; *Junge et al.*, 2005]. However, one must bear in mind that all GrIS topographies tested here are far from flat, and even EEMr3 contains a considerable block of ice of over 2500 m height. Therefore, the Eemian remnant of the GrIS remains a substantial topographic feature with the potential to dam cold low-level air masses west of Greenland, which is fundamental for shaping the atmospheric circulation of the NH high latitudes [*Petersen et al.*, 2004; *Junge et al.*, 2005]. Moreover, comparing the different GrIS sensitivity studies, the response to (partial) Greenland deglaciation seems to be partially model dependent and *Junge et al.* [2005] further reported the dependence on model resolution. Besides, possible far-field effects are likely excluded in this study as the model setup omits the coupling of a dynamic ocean/sea ice module. As shown by *Lunt et al.* [2004] and *Stone and Lunt* [2013], modifications in the GrIS topography also provoke a response in Arctic sea ice, which itself can have an effect on the local surface climate. Thus, repeating the GrIS sensitivity studies performed here with a fully coupled model would be beneficial though computationally expensive.

A focal point of this study is precipitation at pNEEM, i.e., the suggested deposition site of Eemian ice found in the NEEM ice core [*NEEM community members*, 2013]. The Eemian orbital forcing leads to an increase in precipitation (and accumulation) at pNEEM caused by stronger summer precipitation. Changes in the GrIS topography can result in either an additional increase or decrease depending on the actual shape of the GrIS. The precipitation seasonality is enhanced in all experiments indicating that the δ^{18}O isotopic thermometer includes a summer bias for the Eemian. Using the present-day δ^{18}O seasonal cycle (Figure 2 in *Steen-Larsen et al.* [2011] or Figure 6 in *Masson-Delmotte et al.* [2011]), the stronger precipitation seasonality simulated by our model translates into a 0.5–0.8‰ effect on annual mean δ^{18}O corresponding to 1.0–1.6°C warming. This supports the results by *van de Berg et al.* [2013], who found that Eemian condensation temperatures over Greenland likely include a warming signal (up to 2°C), which is unrelated to changes in annual mean SAT. This might at least partially explain the discrepancy between the Eemian δ^{18}O warming estimate of 8 ± 4°C compared to the δ^{15}N estimate of 5°C both recorded at NEEM [*NEEM community members*, 2013]. However, in order to fully understand the δ^{18}O signal, further model experiments including isotope physics are needed, at best also testing the influence of a reduced Eemian GrIS on the moisture transport prior to condensation above pNEEM.

Here the transport routes prior to precipitation events at pNEEM have been studied using Greenland weather patterns and back trajectory analysis. We find that moisture is generally advected from westerly to southerly directions, whereas moisture transport from eastern directions is prohibited as long as pNEEM is located in the lee of the GrIS, which acts as a barrier. However, the scenario of Eemian melting of northeastern Greenland [*Born and Nisancioglu*, 2012] allows moist air masses from the east (Norwegian Sea) to arrive at pNEEM as at least part of the barrier is removed. Hence, such a GrIS topography (EEMr4) would invoke transport-related changes in Eemian sea salt aerosol compositions and deuterium excess in the Eemian NEEM ice, whereas melting of northwestern and southern Greenland would not affect the pNEEM moisture transport. The analysis of aerosol concentrations and deuterium excess in the NEEM record might therefore offer opportunities to judge whether northeastern Greenland was at some point ice-free during the last interglacial. For example, we would expect increased sea salt concentrations if the Eemian GrIS truly looked like EEMr4. This information would be very valuable as currently no data for the Eemian from northeastern Greenland is available.

Note that the major results regarding atmospheric moisture transport to pNEEM drawn from both analysis tools (*k* means clustering and Lagrangian back trajectories) are largely identical. We recommend the cluster analysis of synoptic weather situation as a simple and effective tool to detect major changes in atmospheric moisture transport. The back trajectory analysis on the other hand is more complex but allows a finer analysis. In this regard, a set of more sophisticated criteria relevant for wet deposition of specific chemical species is incorporated in the back trajectory analysis, assessing the detailed transport routes of various aerosols measured in the NEEM core (G. Gfeller et al., manuscript in preparation, 2014).

Furthermore, our results have important implications for modeling the Eemian GrIS extent. The distinct and highly regional precipitation anomalies in response to changed GrIS topography indicate the importance of bidirectional coupling of the ice sheet model with a high-resolution climate model that resolves these regional precipitation changes, which are crucial for a correct representation of the surface mass balance. This also holds for the regional response in summer evaporation and the surface energy balance [*Merz et al.*, 2014], both of which considerably influence the GrIS mass balance. Currently, most ice sheet modeling efforts for the Eemian, including one providing the GrIS topography for this study [*Born and Nisancioglu*, 2012], do not take these important feedback mechanisms into account. With respect to the precipitation response, these studies likely overestimate the GrIS reduction as they ignore the observed precipitation increase over the remaining ice sheet, which has a stabilizing effect. Indeed, *Helsen et al.* [2013], who employ a bidirectional coupling of the ice sheet model with a regional climate model, find limited ice loss in Greenland during the Eemian. Without the important effect of terrain-following precipitation, the surface mass balance of a shrinking GrIS and thus its shape after a period of melting strongly depend on the initial, invariable precipitation patterns of the respective climate models. The results from such ice sheet simulations will at least to some degree reflect biases in the precipitation fields due to, e.g., insufficient resolution. This might explain why simulations of the Eemian GrIS, even if carried out with similar ice sheet code, vary widely when forced by different climate models [*Robinson et al.*, 2011; *Born and Nisancioglu*, 2012]. In summary, the findings presented here suggest that future studies of the GrIS should include a realistic and adaptable representation of local precipitation, either by using high-resolution dynamical downscaling or by developing a suitable parameterization of the relevant effects.

Acknowledgments

We kindly thank Vidya Varma, Matthias Prange, and Alex Robinson for providing data used as boundary conditions in the CCSM4 simulations. We also acknowledge the Swiss National Supercomputing Centre (CSCS) for providing the supercomputing facilities. This is Past4Future contribution 78. The research leading to these results has received funding from the European Union's Seventh Framework program (FP7/2007-2013) under grant agreement 243908, "Past4Future. Climate change—Learning from the past climate" and from the Swiss National Science Foundation, grant "Climate and Environmental Physics." A.B. received financial support from the European Commission under the Marie Curie Intra-European Fellowship ECLIPS (PIEF-GA-2011-300544). The database that this study is based on is too big to made available in a public repository; please contact the authors for specific requests.

References

Bakker, P., et al. (2013), Last interglacial temperature evolution–A model inter-comparison, *Clim. Past*, *9*(2), 605–619, doi:10.5194/cp-9-605-2013.

Bamber, J., J. Griggs, R. Hurkmans, J. Dowdeswell, S. Gogineni, I. Howat, J. Mouginot, J. Paden, S. Palmer, and E. Rignot (2013), A new bed elevation dataset for Greenland, *Cryosphere*, *7*(2), 499–510, doi:10.5194/tc-7-499-2013.

Born, A., and K. H. Nisancioglu (2012), Melting of northern Greenland during the last interglaciation, *Cryosphere*, *6*(6), 1239–1250, doi:10.5194/tc-6-1239-2012.

CAPE Last Interglacial Project Members (2006), Last Interglacial Arctic warmth confirms polar amplification of climate change, *Quat. Sci. Rev.*, *25*(13–14), 1383–1400, doi:10.1016/j.quascirev.2006.01.033.

Chen, Q.-S., D. H. Bromwich, and L. Bai (1997), Precipitation over Greenland retrieved by a dynamic method and its relation to cyclonic activity, *J. Clim.*, *10*(5), 839–870.

Colville, E. J., A. E. Carlson, B. L. Beard, R. G. Hatfield, J. S. Stoner, A. V. Reyes, and D. J. Ullman (2011), Sr-Nd-Pb isotope evidence for ice-sheet presence on southern Greenland during the last interglacial, *Science*, *333*(6042), 620–623, doi:10.1126/science.1204673.

Cuffey, K. M., and S. J. Marshall (2000), Substantial contribution to sea-level rise during the last interglacial from the Greenland ice sheet, *Nature*, *404*(6778), 591–594, doi:10.1038/35007053.

Dansgaard, W., H. B. Clausen, N. Gundestrup, S. J. Johnsen, and C. Rygner (1985), Dating and climatic interpretation of two deep Greenland ice cores, in *Greenland Ice Core: Geophysics, Geochemistry, and the Environment, Geophys. Monogr. Ser.*, vol. 33, edited by C. C. Langway Jr., H. Oeschger, and W. Dansgaard, pp. 71–76, AGU, Washington, D. C, doi:10.1029/GM033p0071.

Dee, D. P., et al. (2011), The ERA-Interim reanalysis: Configuration and performance of the data assimilation system, *Q. J. R. Meteorol. Soc.*, *137*(656), 553–597, doi:10.1002/qj.828.

Dethloff, K., M. Schwager, J. H. Christensen, S. Kilsholm, A. Rinke, W. Dorn, F. Jung-Rothenhausler, H. Fischer, S. Kipfstuhl, and H. Miller (2002), Recent Greenland accumulation estimated from regional climate model simulations and ice core analysis, *J. Clim.*, *15*(19), 2821–2832.

Dethloff, K., W. Dorn, A. Rinke, K. Fraedrich, M. Junge, E. Roeckner, V. Gayler, U. Cubasch, and J. H. Christensen (2004), The impact of Greenland's deglaciation on the Arctic circulation, *Geophys. Res. Lett.*, *31*, L19201, doi:10.1029/2004GL020714.

Draxler, R. R., and G. D. Hess (1998), An overview of the HYSPLIT4 modelling system for trajectories, dispersion and deposition, *Aust. Meteorol. Mag.*, *47*(4), 295–308.

Ettema, J., M. R. van den Broeke, E. van Meijgaard, and W. J. van de Berg (2010), Climate of the Greenland ice sheet using a high-resolution climate model—Part 2: Near-surface climate and energy balance, *Cryosphere*, *4*(4), 529–544, doi:10.5194/tc-4-529-2010.

Evans, K. J., P. H. Lauritzen, S. K. Mishra, R. B. Neale, M. A. Taylor, and J. J. Tribbia (2013), AMIP simulation with the CAM4 spectral element dynamical core, *J. Clim.*, *26*(3), 689–709, doi:10.1175/JCLI-D-11-00448.1.

Gent, P. R., et al. (2011), The Community Climate System Model version 4, *J. Clim.*, *24*(19), 4973–4991, doi:10.1175/2011JCLI4083.1.

Hakuba, M. Z., D. Folini, M. Wild, and C. Schär (2012), Impact of Greenland's topographic height on precipitation and snow accumulation in idealized simulations, *J. Geophys. Res.*, *117*, D09107, doi:10.1029/2011JD017052.

Helsen, M. M., W. J. van de Berg, R. S. W. van deWal, M. R. van den Broeke, and J. Oerlemans (2013), Coupled regional climate-ice-sheet simulation shows limited Greenland ice loss during the Eemian, *Clim. Past*, *9*(4), 1773–1788, doi:10.5194/cp-9-1773-2013.

Hobbs, W. H. (1945), The Greenland glacial anticyclone, *J. Meteorol.*, *2*(3), 143–153.

Hofer, D., C. C. Raible, and T. F. Stocker (2011), Variations of the Atlantic meridional overturning circulation in control and transient simulations of the last millennium, *Clim. Past*, *7*(1), 133–150, doi:10.5194/cp-7-133-2011.

Hofer, D., C. C. Raible, N. Merz, A. Dehnert, and J. Kuhlemann (2012), Simulated winter circulation types in the North Atlantic and European region for preindustrial and glacial conditions, *Geophys. Res. Lett.*, *39*, L15805, doi:10.1029/2012GL052296.

Huth, R., C. Beck, A. Philipp, M. Demuzere, Z. Ustrnul, M. Cahynov, J. Kysel, and O. E. Tveito (2008), Classifications of atmospheric circulation patterns, *Ann. N.Y. Acad. Sci.*, *1146*(1), 105–152, doi:10.1196/annals.1446.019.

Junge, M. M., R. Blender, K. Fraedrich, V. Gayler, U. Luksch, and F. Lunkeit (2005), A world without Greenland: Impacts on the Northern Hemisphere winter circulation in low- and high-resolution models, *Clim. Dyn.*, *24*(2–3), 297–307.

Kahl, J. D. W., D. A. Martinez, H. Kuhns, C. I. Davidson, J. L. Jaffrezo, and J. M. Harris (1997), Air mass trajectories to Summit, Greenland: A 44-year climatology and some episodic events, *J. Geophys. Res.*, *102*(C12), 26,861–26,875, doi:10.1029/97JC00296.

Kopp, R. E., F. J. Simons, J. X. Mitrovica, A. C. Maloof, and M. Oppenheimer (2009), Probabilistic assessment of sea level during the last interglacial stage, *Nature*, *462*(7275), 863–867, doi:10.1038/nature08686.

Kristjansson, J. E., and H. McInnes (1999), The impact of Greenland on cyclone evolution in the North Atlantic, *Q. J. R. Meteorol. Soc.*, *125*(560), 2819–2834, doi:10.1256/smsqj.56002.

Kristjansson, J. E., S. Thorsteinsson, and B. Rosting (2009), Phase-locking of a rapidly developing extratropical cyclone by Greenland's orography, *Q. J. R. Meteorol. Soc.*, *135*(645), 1986–1998.

Lunt, D. J., N. de Noblet-Ducoudre, and S. Charbit (2004), Effects of a melted Greenland ice sheet on climate, vegetation, and the cryosphere, *Clim. Dyn.*, *23*(7–8), 679–694, doi:10.1007/s00382-004-0463-4.

Lunt, D. J., et al. (2013), A multi-model assessment of last interglacial temperatures, *Clim. Past*, *9*(2), 699–717, doi:10.5194/cp-9-699-2013.

Masson-Delmotte, V., et al. (2011), Sensitivity of interglacial Greenland temperature and delta O-18: Ice core data, orbital and increased CO_2 climate simulations, *Clim. Past*, *7*(3), 1041–1059, doi:10.5194/cp-7-1041-2011.

Merkel, U., M. Prange, and M. Schulz (2010), ENSO variability and teleconnections during glacial climates, *Quat. Sci. Rev.*, *29*(1–2), 86–100, doi:10.1016/j.quascirev.2009.11.006.

Merz, N., C. C. Raible, H. Fischer, V. Varma, M. Prange, and T. F. Stocker (2013), Greenland accumulation and its connection to the large-scale atmospheric circulation in ERA-Interim and paleoclimate simulations, *Clim. Past*, *9*, 2433–2450, doi:10.5194/cp-9-2433-2013.

Merz, N., A. Born, C. C. Raible, H. Fischer, and T. F. Stocker (2014), Dependence of Eemian Greenland temperature reconstructions on the ice sheet topography, *Clim. Past*, *10*, 1221–1238, doi:10.5194/cp-10-1221-2014.

Michelangeli, P. A., R. Vautard, and B. Legras (1995), Weather regimes: Recurrence and quasi stationarity, *J. Atmos. Sci.*, *52*(8), 1237–1256.

Neale, R. B., J. Richter, S. Park, P. H. Lauritzen, S. J. Vavrus, P. J. Rasch, and M. Zhang (2013), The mean climate of the Community Atmosphere Model (CAM4) in forced SST and fully coupled experiments, *J. Clim.*, *26*, 5150–5168, doi:10.1175/JCLID-12-00236.1.

Nikolova, I., Q. Yin, A. Berger, U. K. Singh, and M. P. Karami (2013), The last interglacial (Eemian) climate simulated by LOVECLIM and CCSM3, *Clim. Past*, *9*(4), 1789–1806, doi:10.5194/cp-9-1789-2013.

North Greenland Eemian ice drilling project (NEEM) community members (2013), Eemian interglacial reconstructed from a Greenland folded ice core, *Nature*, *493*, 489–494, doi:10.1038/nature11789.

North Greenland Ice Core Project members (2004), High-resolution record of Northern Hemisphere climate extending into the last interglacial period, *Nature*, *431*(7005), 147–151, doi:10.1038/nature02805.

Ohmura, A., and N. Reeh (1991), New precipitation and accumulation maps for Greenland, *J. Glaciol.*, *37*(125), 140–148.

Otto-Bliesner, B. L., S. J. Marsha, J. T. Overpeck, G. H. Miller, A. X. Hu, and C. L. I. P. Mem (2006), Simulating Arctic climate warmth and icefield retreat in the last interglaciation, *Science*, *311*(5768), 1751–1753, doi:10.1126/science.1120808.

Petersen, G. N., J. E. Kristjansson, and H. Olafsson (2004), Numerical simulations of Greenland's impact on the Northern Hemisphere winter circulation, *Tellus A*, *56*(2), 102–111, doi:10.1111/j.1600-0870.2004.00047.x.

Robinson, A., R. Calov, and A. Ganopolski (2011), Greenland ice sheet model parameters constrained using simulations of the Eemian Interglacial, *Clim. Past*, *7*(2), 381–396, doi:10.5194/cp-7-381-2011.

Roe, G. H. (2005), Orographic precipitation, *Annu. Rev. Earth Planet. Sci.*, *33*, 645–671, doi:10.1146/annurev.earth.33.092203.122541.

Schuenemann, K. C., J. J. Cassano, and J. Finnis (2009), Synoptic forcing of precipitation over Greenland: Climatology for 1961–99, *J. Hydrometeorol.*, *10*(1), 60–78, doi:10.1175/2008JHM1014.1.

Sodemann, H., C. Schwierz, and H. Wernli (2008), Interannual variability of Greenland winter precipitation sources: Lagrangian moisture diagnostic and North Atlantic Oscillation influence, *J. Geophys. Res.*, *113*, D03107, doi:10.1029/2007JD008503.

Steen-Larsen, H. C., et al. (2011), Understanding the climatic signal in the water stable isotope records from the NEEM shallow firn/ice cores in northwest Greenland, *J. Geophys. Res.*, *116*, D06108, doi:10.1029/2010JD014311.

Stone, E. J., and D. J. Lunt (2013), The role of vegetation feedbacks on Greenland glaciation, *Clim. Dyn.*, *40*(11–12), 2671–2686, doi:10.1007/s00382-012-1390-4.

Stone, E. J., D. J. Lunt, J. D. Annan, and J. C. Hargreaves (2013), Quantification of the Greenland ice sheet contribution to last interglacial sea level rise, *Clim. Past*, *9*(2), 621–639, doi:10.5194/cp-9-621-2013.

Tsukernik, M., D. N. Kindig, and M. C. Serreze (2007), Characteristics of winter cyclone activity in the northern North Atlantic: Insights from observations and regional modeling, *J. Geophys. Res.*, *112*, D03101, doi:10.1029/2006JD007184.

van de Berg, W. J., M. R. van den Broeke, E. van Meijgaard, and F. Kaspar (2013), Importance of precipitation seasonality for the interpretation of Eemian ice core isotope records from Greenland, *Clim. Past*, *9*(4), 1589–1600, doi:10.5194/cp-9-1589-2013.

Vizcaino, M., W. H. Lipscomb, W. J. Sacks, J. H. van Angelen, B. Wouters, and M. R. van den Broeke (2013), Greenland surface mass balance as simulated by the Community Earth System Model. Part I: Model evaluation and 1850–2005 results, *J. Clim.*, *26*(20), 7793–7812, doi:10.1175/JCLI-D-12-00615.1.

Willerslev, E., et al. (2007), Ancient biomolecules from deep ice cores reveal a forested southern Greenland, *Science*, *317*(5834), 111–114, doi:10.1126/science.1141758.